Biaxial deformation of Ti-6Al-4V and Ti-6Al-4V/TiC composites by transformation-mismatch superplasticity

D.C. Dunand [a,*], S. Myojin [1,b]

[a] Department of Materials Science and Engineering, Massachusetts Institute of Technology, Cambridge, MA 02139, USA
[b] Department of Mechanical Engineering, Massachusetts Institute of Technology, Cambridge, MA 02139, USA

Abstract

Gas-pressure bulge forming of unreinforced Ti-6Al-4V and TiC-reinforced Ti-6Al-4V was performed while cycling the temperature around the allotropic transformation range of the alloy (880–1020°C). The resulting domes exhibited very large strains to fracture without cavitation, demonstrating for the first time the use of transformation-mismatch superplasticity under a biaxial state of stress for both an alloy and a composite. Furthermore, much faster deformation rates were observed upon thermal cycling than for control experiments performed under the same gas pressure at a constant temperature of 1000°C, indicating that efficient superplastic forming of complex shapes can be achieved by transformation-mismatch superplasticity, especially for composites which are difficult to shape with other techniques. However, the deformation rate of the cycled composite was lower than for the alloy, most probably because the composite exhibits lower primary and secondary isothermal creep rates. For both cycled materials, the spatial distribution of principal strains is similar to that observed in domes deformed by isothermal microstructural superplasticity and the forming times can be predicted with existing models for materials with uniaxial strain rate sensitivity of unity. Thus, biaxial transformation-mismatch superplasticity can be modeled within the well-known frame of biaxial microstructural superplasticity, which allows accurate predictions of forming time and strain spatial distribution once the uniaxial constitutive equation of the material is known. © 1997 Elsevier Science S.A.

Keywords: Superplasticity; Deformation; Composites

1. Introduction

Because discontinuously-reinforced metal matrix composites (MMCs) have high strength and low ductility, they are difficult to shape with traditional solid-state forming techniques such as rolling, bending, stamping or forging [1]. Furthermore, their high hardness limits their ability to be machined. Net- and near-net-shape techniques can also be problematic: powder metallurgy processes cannot usually give high dimensional tolerances because of densification shrinkage [1–3], while casting processes can suffer from reinforcement settling in the liquid and/or pushing during solidification [4] and are limited to systems where the liquid matrix shows little reactivity with the environment and the reinforcing phase [5]. Superplastic

forming (a process by which objects with complex shapes can be formed from simple sheets or tubes to large strains with no or limited necking and cavitation) has thus generated strong interest for MMCs [1,6–9]. Much research has been devoted to MMC microstructural superplasticity, where deformation occurs by grain boundary sliding with or without formation of a liquid phase [6,9–11]. An alternative deformation mechanism in unreinforced metals and alloys is mismatch superplasticity, where an external stress biases internal mismatch stresses or strains produced by grains exhibiting an anisotropic coefficient of thermal expansion (CTE) [12–14] or undergoing an allotropic phase transformation [15–17]. This type of superplastic deformation mechanism has also been demonstrated in MMCs, i.e. in Al-SiC composites for which the source of internal mismatch is the CTE difference between matrix and reinforcement (CTE-mismatch superplasticity) [18–21] and, recently, in Ti-TiC composites for which the mis-

match is developed during the matrix allotropic phase transformation (transformation-mismatch superplasticity) [22,23].

Most studies of microstructural or mismatch superplasticity in MMCs focus on uniaxial deformation because it is experimentally simple and easily comparable to existing data. However, superplastic forming processes are characterized by a multiaxial stress state and usually rely on gas-pressure free bulging of sheets in the initial stages of deformation. For a circular sheet, a dome with near-hemispherical shape results, with a balanced biaxial stress state at the apex and a plane-strain state at the equator [24–29]. The main parameters of interest are the time-dependence of the dome height and the thickness distribution within the dome. While gas-pressure bulge forming of domes has been extensively used for unreinforced metals and alloys, only one study, to the best of our knowledge, was performed on MMCs: Chen et al. [30] demonstrated that aluminum reinforced with SiC whiskers could be deformed by CTE-mismatch superplasticity to very large strains and at rates much higher than under isothermal conditions.

The purpose of the present paper is to investigate for the first time biaxial deformation under conditions of transformation-mismatch superplasticity. In the following, we present and discuss experiments of gas-pressure dome bulging of both unreinforced Ti-6Al-4V and Ti-6Al-4V reinforced with TiC particulates performed while cycling the temperature around the phase transformation range of the alloy.

2. Experimental procedures

The materials used were unreinforced Ti-6Al-4V (hot-rolled, annealed rod from President Titanium, MA) and Ti-6Al-4V reinforced with 10 vol.% TiC particulates (cold- and hot-isostatically pressed CermeTi-10™ sheet [31,32] from Dynamet Technology, MA). The Ti-6Al-4V rod (diameter, 41.1 mm) was machined into a cylinder (wall thickness, 2.38 mm; length, 16.6 mm) with one end as a solid 2.24 mm thick disk. A disk of the same thickness was machined from the Ti-6Al-4V/TiC composite sheet and welded at the other end of the cylinder, thus forming a closed chamber to which a Ti-3Al-2.5V tube (diameter, 6.35 mm) was welded to allow gas pressurization and access for a thermocouple. To determine radial and hoop strains, the disks were lightly scribed with concentric fiducial circles spaced 1 mm apart and crossed by three perpendicular sets of parallel fiducial lines going through the center of the disk. The chamber was introduced into a boron-nitride coated stainless steel sleeve (2.5 mm thick), preventing radial deformation of the cylinder but allowing axial deformation of both reinforced and

unreinforced end disks with a free diameter of 33.4 mm (Fig. 1) [33]. The chamber assembly was outfitted with two K-type thermocouples in contact with the inside surface of the titanium tube (to which temperature are referred in the following) and the outside surface of the steel sleeve, respectively. The assembly was placed in the center of a cylindrical graphite furnace within a stainless steel vessel and oriented such that two of the fiducial line sets were vertical and one horizontal.

Both vessel and test chamber were evacuated to 10 mTorr, flushed with 99.9996% pure argon and evacuated again to 10 mTorr. The furnace was then heated to 150°C for about 10 h to allow degassing and ramped to 350, 600 and 800°C with degassing hold periods of 1 h at each temperature; a dynamic vacuum of about 10 mTorr was conserved throughout the experiment and the oxygen contamination of the sample was further reduced by titanium foil getters. For the isothermal experiment, the temperature was raised to 1000°C and the test chamber and vessel were pressurized with 99.9996% pure argon to a pressure of 350 and 120 kPa, respectively, leading to the simultaneous outward bulging of both reinforced and unreinforced disks under a net gas pressure of 230 kPa. The experiment was conducted at constant temperature and pressure until failure of one of the disks. For the cycling experiments, the same gas pressures were used but the temperature was cycled between 880 and 1020°C with a period of 600 s (with ramps of about 60 s), until failure of the chamber. For these conditions, Szkliniarz and Smolka
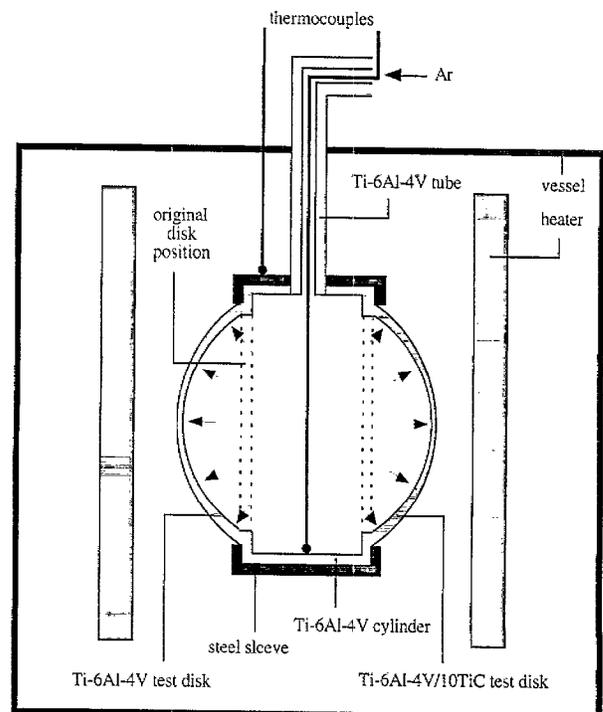

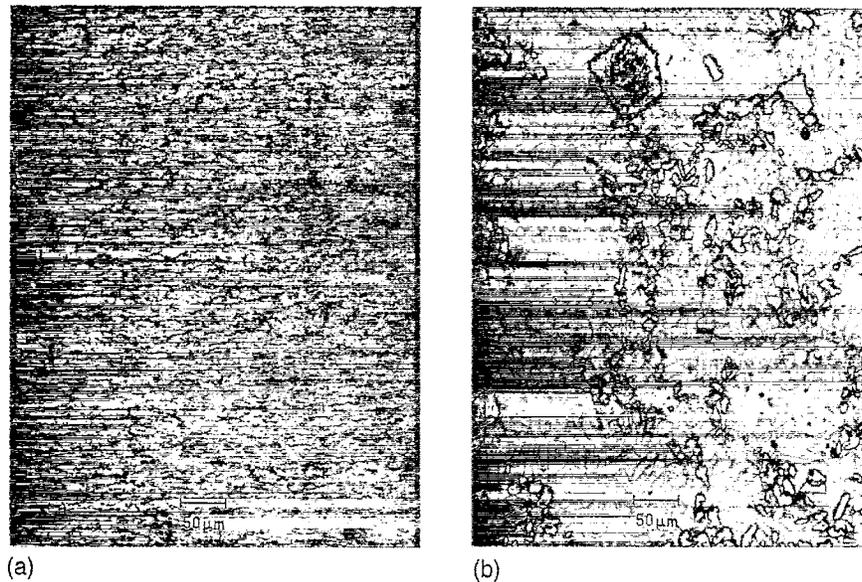Fig. 1. Schematic drawing of experimental apparatus.

Fig. 2. Micrographs of undeformed materials. (a) Unreinforced Ti-6Al-4V (rolling direction is horizontal); (b) TiC-reinforced Ti-6Al-4V.

[34] predict that the volume fraction of β phase varies between about 20% at the lowest temperature and about 100% at the highest temperature. By connecting the chamber to an argon reservoir at constant temperature, the temperature-induced pressure fluctuation were reduced to ± 5 kPa. In a first cycling experiment, both reinforced and unreinforced disks were allowed to deform simultaneously, while in a second cycling experiment, the unreinforced disk was supported by a steel insert to prevent deformation, so that only the reinforced disk was free to deform. Except for the second cycling experiment, the experiments were interrupted after 10 h by a short excursion to room temperature to allow visual inspection of the samples. The principal strains were determined after deformation by measuring the thickness of the dome as a function of distance from the apex with a point micrometer, and the distance between the fiducial marks with a traveling microscope. For all strains, three sets of measurements were performed along the three sets of radial lines at right angles to each other.

3. Results

Fig. 2(a,b) shows the microstructure of the Ti-6Al-4V and Ti-6Al-4V/TiC materials before thermal cycling. In both samples, the metallic phase consists of α-grains separated by an intergranular β-phase. In unreinforced Ti-6Al-4V, the α-grains are elongated (approximate aspect ratio, 4) and oriented in the rolling direction, while in the composite material, the α-grains have an aspect ratio of about 2 and are randomly oriented. In both cases, the smallest α-grain dimension is about 10 μm. The angular, equiaxed TiC reinforcement exhibits

a broad size distribution between about 10 and 100 μm (Fig. 2(b)).

Table 1 summarizes the main experimental conditions and results for all experiments. The isothermal experiment no. 1 was stopped upon failure of the Ti-6Al-4V weld, while the cycling experiment no. 2 was interrupted when the apex of the Ti-6Al-4V dome developed four cracks less than 1 mm in length. Because of the extensive deformation of the dome in experiment no. 2, the apex came in contact with the graphite furnace and the fracture was thus most probably induced by the embrittlement resulting from carbon diffusion and/or by overheating at the point of contact. For both isothermal and cycling experiments, the unreinforced dome exhibited a larger deformation than the reinforced dome. Finally, cycling experiment no. 3, for which only the reinforced disk was allowed to bulge, also terminated upon contact of the dome apex with the graphite furnace and formation of a small, millimeter-long crack at the apex. Density measurements performed by the Archimedes method on the full domes showed, within experimental error, no change in overall density after deformation.

Fig. 3(a–c) shows the deformed domes after separation from the chamber. For comparable total deformation times, thermal cycling leads to a much larger deformation than isothermal holding for both the unreinforced alloy (Fig. 3(a)) and the composite (Fig. 3(b)). Fig. 3(c) shows the Ti-6Al-4V and Ti-6Al-4V/TiC domes deformed to fracture by thermal cycling and illustrates the extensive deformation achievable by transformation-mismatch superplasticity. It also shows that the total strain to fracture and the deformation rate are larger in the unreinforced alloy than in the composite, despite the larger number of cycles experienced by the latter specimen.

Table 1
Experimental results and theoretical predictions for all samples

Sample	No.	Fracture location	Maximum equivalent true strain at apex	Maximum equivalent stress (MPa)	Total cycle number	Observed deformation time (ks)	Predicted deformation time[a] (ks)	Predicted deformation time[b] (ks)
Isothermal								
Ti-6Al-4V	1.1	Weld	0.33	1.3	—	55.8	—	—
—Ti-6Al-4V/TiC	1.2	— ⁻ ⁻	0.32	1.3	—	55.8	—	—
Cycling								
Ti-6Al-4V	2.1	Apex	2.6	14.6	101	60.6	108	61.7
Ti-6Al-4V/TiC	2.2	—	0.64	1.6	101	60.6	74.0	67.2
Ti-6Al-4V/TiC	3.0	Apex	2.1	8.2	147	88.2	125	104

[a] Eq. (4) without primary contribution.
[b] Eq. (4) with primary contribution.

The principal true strains are plotted as a function of the original distance from the disk center for the unreinforced specimen no. 2.1 deformed to fracture in Fig. 4(a) and for the corresponding composite specimen no. 2.2 subjected to the same number of cycles in Fig. 4 (b). For each principal strain, the scatter between the three sets of strain measurements is due to the uneven dome shape resulting from the gravitational force on the domes during the experiment. As seen in Fig. 1, the undeformed disks were vertical, so that the bulged domes sagged in an uneven manner under their own weight. Systematic errors were reduced by the spatial orientation of the fiducial lines: for each principal strain, the two vertical sets of strain measurements gave maximum and minimum values and the third horizontal set of measurements gave average values. A reasonable fit is found for each principal strain by fitting linearly all three sets of measurements. Fig. 5 shows the thickness strain as a function of the original distance from the disk center for both materials tested to fracture (samples 2.1 and 3, the latter with only one full and one partial set of data points).

4. Discussion

4.1. Superplastic deformation

Fig. 3(a–c) demonstrate for the first time that biaxial deformation is possible by transformation-mismatch superplasticity. Dome bulge forming under thermal cycling about the allotropic temperature range of unreinforced Ti-6Al-4V and TiC-reinforced Ti-6Al-4V is characterized both by very large strains to fracture without cavitation and by deformation rates faster than during isothermal deformation at the highest cycle temperature of the control unreinforced alloy. We note however that the absolute rates of deformation measured in the present study are much lower than the values $(10^{-4}–10^{-3}$ s$^{-1})$ achieved with microstruc-

turally superplastic Ti-6Al-4V specimens which were thermo-mechanically processed for optimal grain size (about 6 μm) and deformed at the optimum forming temperature of about 930°C [24]. For the isothermal experiments in the present study, this is because the initial grain size (Fig. 2(a)) is significantly larger than the optimal value of about 6 μm and because the testing
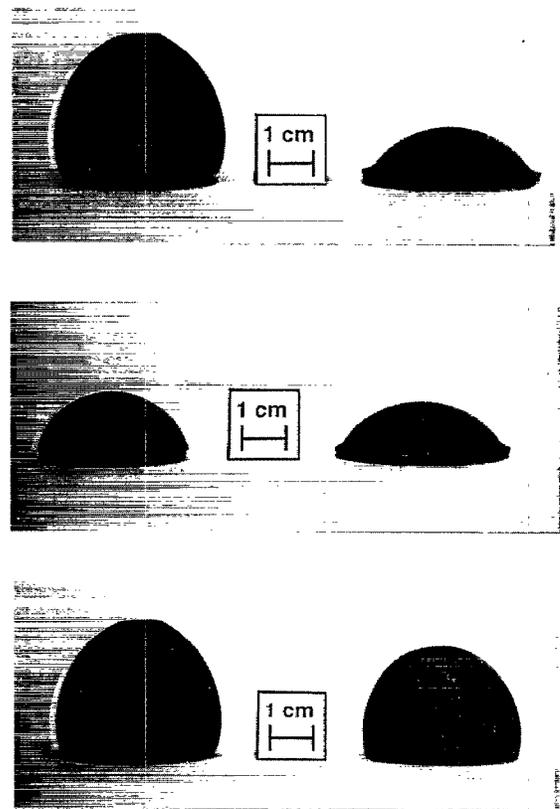

Fig. 3. Deformed domes. (a) Unreinforced Ti-6Al-4V: cycled (left, sample 2.1) and isothermal (right, sample 1.1); (b) composite Ti-6Al-4V/TiC: cycled (left, sample 2.2) and isothermal (right, sample 1.2); (c) Samples cycled to fracture: unreinforced Ti-6Al-4V (left, sample 2.1) and Ti-6Al-4V/TiC (right, sample 3).

took place above the β-transus temperature where rapid grain growth occurs. For the cycling experiments in the present study, the deformation rates were limited by the large thermal mass of the steel sleeve which precluded more rapid cycling.

However, for temperature cycling frequencies five times higher than in the present paper, an average uniaxial strain rate of 5×10^{-5} s^{-1} has been measured (Zwigl and Dunand, unpublished research) for both Ti-6Al-4V and TiC reinforced Ti-6Al-4V specimens deforming by transformation superplasticity under a uniaxial stress of 4 MPa. A combination of higher applied stresses and faster temperature cycling with radiant or sample resistance heating may allow further increases in the average strain rate by about an order of magnitude, resulting in deformation rates comparable to those achievable with optimized Ti-6Al-4V materials exhibiting microstructural superplasticity. Thus, forming of complex shapes by transformation-mismatch superplasticity could become an attractive net-shape processing method, especially for titanium-based composites which are difficult to roll and forge (because of the brittleness of the reinforcement), machine (because of the hardness of the reinforcement) or cast (because of the reactivity of the matrix). Alternatively, transformation superplasticity could be used for allotropic titanium alloys such as Ti-6Al-4V when economical or technological reasons preclude the complex thermo-mechanical process leading to the fine-grained structure necessary for microstructural superplasticity, e.g. for near-net-shape, as-cast or powder-metallurgy items.

As discussed in more detail in an earlier publication [23], the mismatch developed during the phase transformation of titanium is significantly larger than the CTE mismatch between Ti and TiC for a given temperature cycling range. Hence, while transformation-mismatch superplasticity is inherently restricted to allotropic materials, the achievable deformation rate is higher than for CTE-mismatch superplasticity. Other systems for which transformation mismatch superplasticity is of interest include allotropic metals and alloys (e.g. iron, cobalt and zirconium), intermetallics (e.g. MoSi$_2$, Cr$_2$Nb), ceramics (e.g. zirconia, hafnia, tungsten boride and tantalum carbide) and composites containing at least one of these allotropic constituents [23,35].

The smaller dome deformation observed in the composite as compared to the unreinforced alloy (samples 2.1 and 2.2, Fig. 3(c)) is unexpected, since previous uniaxial cycling experiments on unalloyed titanium with and without 10 vol.% TiC particulates resulted in larger uniaxial deformation rates for the composite, an effect modeled by considering the increased mismatch stresses in the composite [23]. Three possible explanations can be advanced for this discrepancy. First, we note that the peak internal mismatch stresses between matrix and reinforcement are expected to be smaller for Ti-6Al-4V

than for unalloyed titanium, because relaxation during transformation can occur over the whole 830–980°C [34] transformation range of Ti-6Al-4V, as compared to the single transformation temperature of 882°C for Ti. Second, isothermal creep deformation is slightly slower for the composite than for the alloy, as illustrated by the isothermal experiments where the maximum dome strain and dome height are somewhat smaller for the composite than for the unreinforced sample. Thus, the isothermal creep contribution during the high-temperature hold period of the cycle is expected to be larger for the unreinforced dome, especially for large dome deflections when the stresses in the dome are high. Third, as
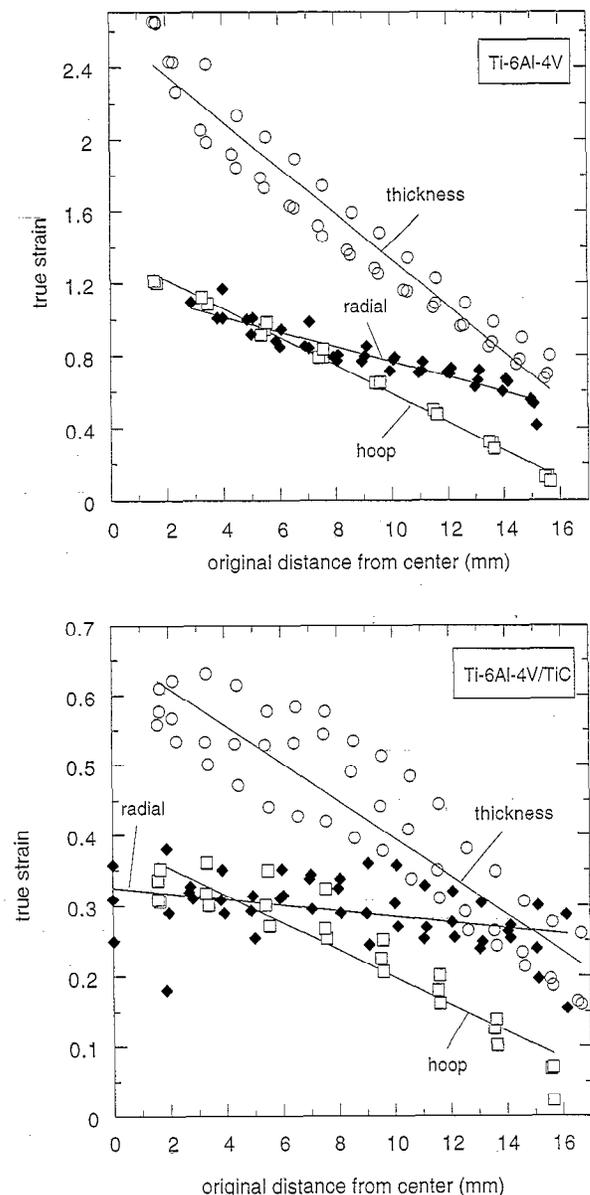

Fig. 4. Absolute value of the three principal strains as a function of the original distance from the disk center. (a) Ti-6Al-4V deformed to fracture (sample 2.1). (b) Ti-6Al-4V/TiC deformed for the same number of cycles (sample 2.2).
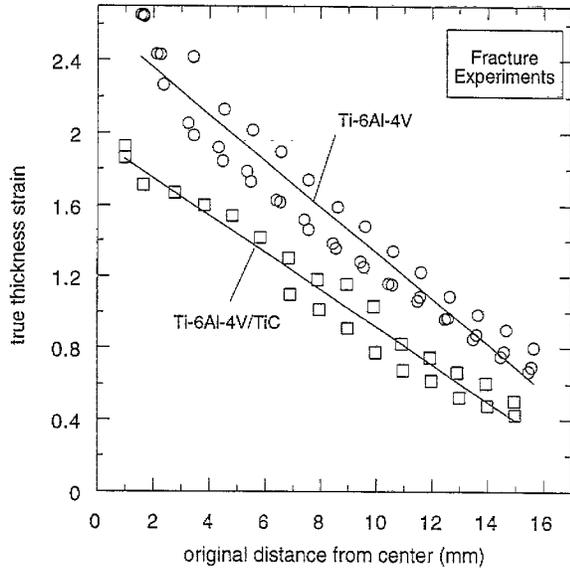
Fig. 5. Absolute value of the thickness strain as a function of the original distance from the disk center for Ti-6Al-4V deformed to fracture (sample 2.1) and for Ti-6Al-4V/TiC deformed to fracture (sample 3).

discussed in more details later, the contribution of primary creep during the initial thermal cycles is much higher for the unreinforced alloy than for the composite.

4.2. Deformation time

Considering the biasing of internal strains by an externally applied uniaxial stress σ and using the von Mises criterion, Greenwood and Johnson [15] derived a relationship for the uniaxial strain $\Delta\varepsilon_t$ due to transformation-mismatch plasticity over a full temperature cycle:

$$\Delta\varepsilon_t = \frac{5}{3}\frac{\Delta V}{V}\frac{\sigma}{\sigma_y} \tag{1}$$

where $\Delta V/V$ is the fractional constrained volume change during the transformation and σ_y is the uniaxial yield stress of the weakest phase at the transformation temperature. Neglecting isothermal creep taking place during the cycle, an average strain-rate $\bar{\dot\varepsilon}$ can be defined by multiplying the transformation strain $\Delta\varepsilon_t$ given in Eq. (1) by the cycling frequency v. Rearranging Eq. (1) gives:

$$\sigma = \frac{\sigma_0}{\dot\varepsilon_0}\cdot\bar{\dot\varepsilon} \tag{2}$$

corresponding to a constitutive uniaxial creep equation with a strain-rate sensitivity of unity and a proportionality constant $\sigma_0/\dot\varepsilon_0$ given by:

$$\frac{\sigma_0}{\dot\varepsilon_0} = \frac{3}{5v}\cdot\frac{\sigma_y}{\Delta V/V} \tag{3}$$

For unreinforced Ti-6Al-4V, Kot et al. [36] found values of $v\cdot\sigma_0/\dot\varepsilon_0 = 310$ MPa for very rapid cycles ($v = 120$ h^{-1}) between 760 and 980°C, while Zwigl and Dunand (unpublished research) found $v\cdot\sigma_0/\dot\varepsilon_0 = 225 \pm 25$ MPa for Ti-6Al-4V and $v\cdot\sigma_0/\dot\varepsilon_0 = 280 \pm 50$ MPa for Ti-6Al-4V/TiC for cycle frequencies and temperature range ($v = 2.5$–10 h^{-1}, $T = 860$–1020°C) comparable to those used in the present study ($v = 6$ h^{-1}, $T = 880$–1020°C).

For a material deforming according to Eq. (2), Ragab [37] derived a closed-form solution for the time t^* necessary to deform a flat disk into a dome of height Y_b:

$$t* = \frac{\sigma_0}{p}\frac{h_0}{b_0}\left[\frac{Y}{(1+Y^2)} - \frac{2Y}{(1+Y^2)^2} + \tan^{-1}Y\right] \tag{4}$$

where p is the gas pressure, h_0 the initial disk thickness, b_0 the initial disk radius and $Y = Y_b/b_0$ the relative height of the dome.

The values predicted by Eq. (4) and the corresponding experimental values are listed in Table 1; the predicted values are significantly higher than the observed values. The likeliest explanation for this discrepancy is the contribution of primary creep during transformation-mismatch superplasticity which is significant for the first 50 cycles in unreinforced Ti-6Al-4V (Zwigl and Dunand, unpublished research). Averaging the total (sum of primary and secondary) uniaxial strain rate over 101 cycles (corresponding to the number of cycles of experiment 2), the uniaxial proportionality constant $v\cdot\sigma_0/\dot\varepsilon_0$ is 390 MPa (Zwigl and Dunand, unpublished research), leading to a value of $t^* = 61.7$ ks in good agreement with the measured value of 60.6 ks (Table 1). For the composite, the primary regime is much shorter as it extends over only about 20 cycles (Zwigl and Dunand, unpublished research), leading to corrected times t^* in reasonable agreement with the measured values (Table 1), given the uncertainties in measurement and the many simplifying assumptions used.

4.3. Strain Distribution

Fig. 4 (a–b) show that the three principal true strains vary linearly with the original distance from the disk center, as also observed in other bulge experiments of microstructurally superplastic alloys [26,28,37]. At the dome equator, the hoop strain e_h is within experimental errors equal to zero while the thickness strain e_t and radial strain e_r are equal, as expected for a plane-strain state. Conversely, at the dome apex, the hoop and radial strains are nearly equal and half the value of the thickness strain, as expected for an equibiaxial stress state. These observations further illustrate that the behavior of materials deformed by transformation-mismatch superplasticity is similar to that of
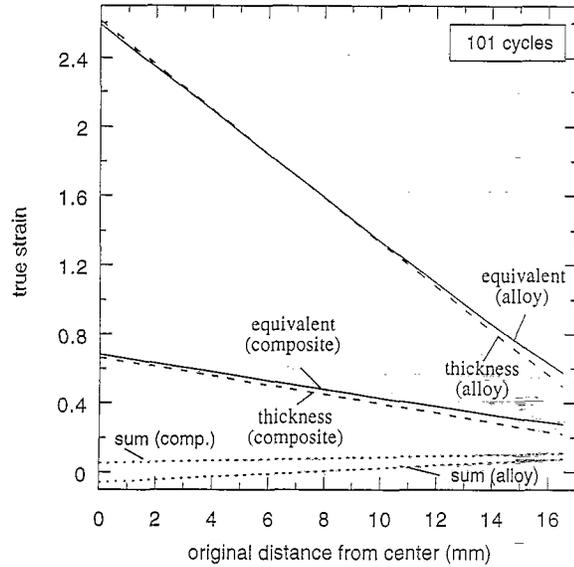
Fig. 6. Thickness strain (best-fit line in Fig. 4), equivalent strain (calculated with Eq. (5) from the best-fit lines in Fig. 4) and sum of principal strains (calculated from the best-fit lines from Fig. 4) for Ti-6Al-4V deformed to fracture (sample 2.1) and for Ti-6Al-4V/TiC deformed for the same number of cycles (sample 2.2).

microstructurally-superplastic materials. In Fig. 6, the best fit lines from Fig. 4(a)–(b) for the thickness strain measurements e_t is replotted for both materials, together with the calculated von Mises equivalent strain $\bar{e}$:

$$\bar{e} = \frac{\sqrt{2}}{3} [(e_r - e_h)^2 + (e_h - e_t)^2 + (e_t - e_r)^2]^{1/2} \qquad (5)$$

The equivalent strain, which varies nearly linearly between a minimum value at the equator $(\bar{e} = e_t)$ and a maximum value at the apex $(\bar{e} \cong 2/\sqrt{3}\, e_t = 1.15 \cdot e_t)$ is equal to the thickness strain e_t within experimental error. Also plotted in Fig. 6 is the sum of the three principal strains, which is close to zero as expected from volume conservation, thus demonstrating that the strain measurements are accurate.

The thickness strains (roughly equal to the equivalent strains, as shown above) are compared in Fig. 5 for the experiments conducted to fracture. As for the unreinforced alloy, the composite shows a linear relationship between strain and original distance from the disk center, indicating that the flow behavior of the composite deformed to fracture is similar to that observed in materials deformed under microstructural superplasticity conditions. The equivalent true strains experienced by the unreinforced and reinforced materials deformed to fracture are bounded by the minimum values at the equator (about 0.64 and 0.60, respectively) and the maximum values at the apex (about 2.6 and 2.1, respectively, Table 1). Despite the very high values

of strains throughout the dome, no change in average density was recorded after superplastic deformation, indicating that these materials are resistant to cavitation when deformed by transformation-superplasticity. Further work is however needed to examine the mechanisms of pore nucleation and growth during transformation-mismatch superplasticity, as well as the geometry of fracture at the necking point.

The maximal strain and stress values are found at the dome apex, where the state of stress is balanced biaxial. Table 1 lists the apex average von Mises equivalent strains (calculated as twice the hoop or radial strain determined experimentally over an initial apex area of 4-11 mm²) and the corresponding maximum equivalent stresses, equal to the tangential or radial stress and calculated from [28]:

$$\bar{\sigma} = \frac{p}{4} \frac{b_0}{h} (Y + Y^{-1}) \qquad (6)$$

where h is the average thickness at the apex calculated from the initial thickness h_0 and the average measured equivalent strain. The maximum equivalent strains reached in the isothermal experiments (true strain of 0.33, corresponding to an engineering strain of about 38%) are too low to be labeled as superplastic. On the other hand, the maximum equivalent strains reached by both the unreinforced alloy and the composite (2.6 and 2.1, or engineering values of 1250 and 720%, respectively) are very high and typical of superplastic materials. The corresponding equivalent stresses (Eq. (6), Table 1) are high enough to induce rapid creep at the highest temperature of the cycle [38]. It is thus likely that isothermal creep contributed significantly to cavitation of the fractured samples and that higher fracture strains could be reached if the stress is maintained in the optimal stress window for transformation-mismatch superplasticity.

5. Conclusions

● Very large equivalent true strains have been demonstrated in Ti-6Al-4V (up to 2.6) and Ti-6Al4V reinforced with 10 vol.% TiC particulates (up to 2.1) by gas-pressure dome bulging during thermal cycling around the phase transformation of the alloy. To the best of our knowledge, this is the first report of transformation-mismatch superplasticity under a biaxial stress state.

● For both the unreinforced alloy and the metal matrix composite, the deformation rate upon thermal cycling (880–1020°C) was much faster than upon isothermal creep near the upper temperature of the cycle (1000°C). Furthermore, average dome density measurements did not indicate any cavitation within measurement accuracy. Thus, superplastic forming of

complex shapes by transformation-mismatch super-plasticity could become an attractive net-shape processing method for allotropic materials, especially for composites which are difficult to shape by traditional forming techniques or for composites and alloys which cannot be thermomechanically processed to induce microstructural superplasticity.

- The deformation rate by transformation-mismatch superplasticity was lower for the composite than for the unreinforced alloy. This is probably due to the higher strength of the composite which exhibits both a reduced average primary creep rate during thermal cycling and a reduced isothermal secondary creep rate as compared to the unreinforced alloy.

- The three principal strains and the von Mises equivalent strain decrease linearly as a function of distance between the dome apex, where an equibiaxial state of stress is observed, and the dome equator, where plane-strain conditions are found. These findings are similar to those reported for materials deforming by microstructural superplasticity, indicating that biaxial transformation-mismatch superplasticity can be described with existing models for biaxial microstructural superplasticity. This is confirmed by the reasonable agreement found between the measured deformation times and those predicted by Ragab [37] for materials with strain sensitivity of unity.

References

[1] A.K. Ghosh, in: S. Suresh, A. Mortensen and A. Needleman (Eds.), *Fundamentals of Metal Matrix Composites*, Butterworth–Heinemann, Boston MA, 1993, p. 23.

[2] E.K.H. Li, P.D. Funkenbusch, Metall. Trans. 24A (1993) 1345.

[3] N. Taylor, D.C. Dunand, A. Mortensen, Acta Metall. Mater. 41 (1993) 955.

[4] A. Mortensen, I. Jin, Intern. Mater. Rev. 37 (1992) 101.

[5] V.J. Michaud, in: S. Suresh, A. Mortensen and A. Needleman (eds.), *Fundamentals of Metal Matrix Composites*, Butterworth–Heinemann, Boston MA, 1993, p. 3.

[6] T.G. Nieh, J. Wadsworth, Mater. Sci. Eng. A147 (1991) 129.

[7] D.C. Dunand and B. Derby, in: S. Suresh, A. Mortensen and A. Needleman (eds.), *Fundamentals of Metal Matrix Composites*, Butterworth–Heinemann, Boston MA, 1993, p. 191.

[8] R.S. Mishra, T.R. Bieler, A.K. Mukherjee, Acta Metall. Mater. 43 (1995) 877.

[9] M. Mabuchi, H. Iwasaki, K. Higashi, T.G. Langdon, Mat. Sci. Technol. 11 (1995) 1295.

[10] J. Pilling, Scripta Metall. 23 (1989) 1375.

[11] T.G. Nieh, T. Imai, J. Wadsworth, S. Kojima, Scripta Metall. Mater. 31 (1994) 1685.

[12] W. Boas, R.W.K. Honeycombe, Proc. R. Soc. London 188A (1947) 427.

[13] M.Y. Wu, J. Wadsworth, O.D. Sherby, Metall. Trans. 18A (1987) 451.

[14] S.M. Pickard, B. Derby, Scripta Metall. Mater. 25 (1991) 467.

[15] G.W. Greenwood, R.H. Johnson, Proc. R. Soc. London 283A (1965) 403.

[16] M. de Jong, G.W. Rathenau, Acta Metall. 7 (1959) 246.

[17] M. Zamora, J.P. Poirier. Mech. Mater. 2 (1983) 193.

[18] M.Y. Wu, O.D. Sherby, Scripta Metall. 18 (1984) 773.

[19] G.S. Daehn, G. Gonzalez-Doncel, Metall. Trans. 20A (1989) 2355.

[20] S.M. Pickard, B. Derby, Acta Metall. Mater. 38 (1990) 2537.

[21] J.A.G. Furness, T.W. Clyne, Mater. Sci. Eng. A141 (1991) 199.

[22] C.M. Bedell, P. Zwigl and D.C. Dunand, in: A.K. Ghosh and T.R. Bieler (Eds.), *Superplasticity and Superplastic Forming*, TMS, Warrendale PA, 1995, p. 125.

[23] D.C. Dunand, C.M. Bedell, Acta Mater. 44 (1996) 1063.

[24] J. Pilling and N. Ridley, *Superplasticity in Crystalline Solids*, The Institute of Metals, London, 1989.

[25] C.F. Yang, L.H. Chiu, S.C. Lee, Scripta Mater. 34 (1996) 1555.

[26] A.K. Ghosh, C.H. Hamilton, Metall. Trans. 13A (1982) 733.

[27] Z.X. Guo, N. Ridley, Mater. Sci. Eng. A114 (1989) 97.

[28] Z.X. Guo, N. Ridley, Mater. Sci. Technol. 6 (1990) 510.

[29] A. Dutta, A.K. Mukherjee, Mater. Sci. Eng. A157 (1992) 9.

[30] Y.C. Chen, G.S. Daehn, R.H. Wagoner, Scripta Metall. Mater. 24 (1990) 2157.

[31] S. Abkowitz, P.F. Weihrauch, Adv. Mater. Proc. 136 (7) (1989) 31.

[32] S. Abkowitz, P.F. Weihrauch, S.M. Abkowitz, H.L. Heussi, J. Metals 47 (8) (1995) 40.

[33] S. Myojin, *BS Thesis*, Department of Mechanical Engineering, Massachusetts Institute of Technology, 1995.

[34] W. Szliniarz, G. Smolka, *J. Mater. Proc. Tech.*, (1995) 413.

[35] D.C. Dunand and C.M. Bedell, U.S. *Patent No. 5413649*, 1995.

[36] R. Kot, G. Krause and V. Weiss, in: R.I. Jaffe and N.E. Promisel (Eds.), *The Science, Technology and Applications of Titanium*, Pergamon, Oxford, 1970, p. 597.

[37] A.R. Ragab, Metals Technol. 10 (1983) 340.

[38] H. Oikawa, K. Nishimura, M.X. Cui, Scripta Metall. 19 (1985) 825.